THE CAMBER DISTRIBUTION OF A SPANWISE UNIFORMLY LOADED SUBSONIC WING

Toshio Kawasaki, Masao Ebihara

NASA TT F-10,781

Technical Report TR-104, National Aerospace Laboratory, Tokyo, pp. 1-23, 1966.

NATIONAL AERONAUTICS AND SPACE ADMINISTRATION
WASHINGTON D.C. 20546 MARCH 1967

THE CAMBER DISTRIBUTION OF A SPANWISE UNIFORMLY LOADED SUBSONIC WING*

Toshio Kawasaki**, Masao Ebihara**

ABSTRACT. In this report the author discusses the shape of three-dimensional wings in subsonic flow, with a load distribution uniform in spanwise- and arbitrary in chordwise-direction. A certain restriction has to be placed on the planform of the wing: the wing, swept-back or not, should have straight leading- and trailing-edges.

Formulas derived from linearized theory are given, with which one can obtain the camber shape from predetermined load distribution.

In addition, an expression for calculating the Mach number distribution normal to the isobars on the wing surface is presented.

Some numerical examples show that the advent of the critical stage on the wing surface will be delayed up to a considerably high free-stream Mach number by designing the camber shape for the wing in such a manner that it possesses spanwise uniform loading with a chordwise shape suitable for the distribution.

/1***

1. Introduction

The reason for the fact that many airplanes having high subsonic or supersonic cruising speeds have swept-back wings is that it can increase the critical Mach number on the wing surface. In other words, it can suppress the generation of shock waves up to higher Mach numbers.

According to Bickley (Ref. 1), shock waves will be generated when the velocity component normal to the isobars exceeds local sonic speed in the flow-field at a certain point on the wing. Therefore, this velocity component should be reduced in order to delay the generation of shock waves. For this purpose, the angle between the direction of velocity and the isobar line is to be reduced, taking advantage of the swept-back angle.

In the case of a swept-wing having an infinite span, all isobar lines on the wing have the same angle with the main stream as the front edge makes with it. Hence, the critical Mach number increases proportionally with the sine of this angle, when compared with the corresponding two-dimensional wing. /2

However, in the case of a three-dimensional wing having a finite span, a

---

* March 29, 1966.

** Aerodynamics Department II.

*** Numbers in the margin indicate pagination in foreign text.

swept-back angle does not simply result in the inclination of isobars. Especially at the base and tip of the wing, the isobars tend to become normal to the main stream, thus loosing the effect of the sweep-back angle almost entirely (Ref. 2).

In order to prevent this, it is possible to modify the outline for the cross section of the wing so as to make the isobars at the tip and base of the wing approach those of the infinite-span swept-wing.

Based on this idea, Kuchemann (Ref. 3) and Weber (Ref. 4) considered the thickness and camber distribution of a wing cross section for a semi-infinite span, swept-back wing.

In this report, we computed the camber distribution for a finite-span wing with a uniform span-wise load distribution. The considered outline of the wing possesses straight-line leading and trailing edges with a possible taper.

When the span-wise load distribution is uniform, the isobars become straight lines passing through the intersection of the extensions of the leading and trailing edges, so that the direction normal to the isobars makes a larger angle with the main stream than the swept-back angle of the trailing edge. Thus, a sufficient swept-back angle effect can be expected at the tip and base of the wing.

In order to confirm this effect, it is necessary to obtain the flow field on the wing having the computed camber distribution and to find the distribution of Mach number component normal to the isobars in the direction of the wing chord. For this purpose, we derived equations giving the Mach number component normal to the isobar.

Symbols

a: Refer to Figure 2. It represents the local sonic speed in (Ref. 8);
a_∞: Sonic speed of uniform stream;
AR: Aspect ratio;
b: Refer to Figure 2;
c_p: Pressure coefficient;
c_{PU}: $\lim_{z\to 0+} c_p$ pressure coefficient above the upper surface;
c_{PL}: $\lim_{z\to 0-} c_p$ pressure coefficient below the lower surface;
$l(x_1,y_1)$: Load distribution. Refer to (2.4);
l_{1a}: Refer to (4.1);
l_{2b}: Refer to (4.2);
M: Local Mach number;
M_∞: Mach number of uniform stream; /3
M_n: Mach number component normal to isobars;
r: $r=\sqrt{(x-x_1)^2+(y-y_1)^2+z^2}$

s: Half wing-span (when the chord length at the wing base is made 1);
V: Velocity of uniform stream;
V_n: Velocity component normal to isobars;
v_x: Velocity disturbance in x-direction;
v_y: Velocity disturbance in y-direction;
v_z: Velocity disturbance in z-direction;
x: Coordinate in the direction of uniform stream;
x_1: Variable of integration in x-direction;
x_ℓ: Equation of leading edge; refer to (3.1);
x_{r1}: $x_{r1} = x-1-s \tan \psi$;
x_{ra}: $x_{ra} = x-a-s \tan \chi$;
x_{rb}: $x_{rb} = x-b-s \tan \Omega$;
$x_{x\xi_1}$: $x_{x\xi_1} = x-\xi_1-s \tan \Lambda_{\xi_1}$;
x_t: Equation of trailing edge. Refer to (3.2);
y: Coordinate normal to uniform stream on the wing surface;
y_1: Variable of integration in y-direction;
z: Coordinate in the direction normal to the wing surface;
z_c: Camber distribution. Refer to (7.1);
z_{cm}: Camber distribution. Refer to (7.3);
z_t: Thickness distribution;
α: local elevation angle. Refer to (7.2);
ξ: Ratio of the distance from the front edge to the local chord length. Refer to (4.3);
ξ_1: Variable of integration of ξ;
Λ: Angle between isobar and y-axis;
Λ_ξ: Refer to Figure 1;
Λ_{ξ_1}: Refer to (5.3);
λ: 1 - (taper ratio);
ρ: $\rho = s/\lambda$;
σ: $\sigma = \lambda/s$;
$\tau(x_1,y_1)$: Intensity of doublet placed at the point (x_1, y_1); /4
$\phi(x,y,z)$: Disturbance potential;
φ: Sweep-back angle of leading edge;
ψ: Sweep-back angle of trailing edge;
χ: Refer to (6.6);
Ω: $\tan^{-1}(\tan \varphi - \sigma b)$;
$1(x)$: Refer to (4.5).

Suffix:

c: Quantities in incompressible flow.

2. Fundamental Equations

According to the linear theory of incompressible gases, the disturbance potential due to a wing having a camber, but no thickness, which is placed in a stream at a small elevation angle, is given by the following equation

$$\phi(x,y,z)=-\frac{1}{4\pi}\iint_{S+W}\tau(x_1,y_1)\frac{\partial}{\partial z}\left(\frac{1}{r}\right)dx_1dy_1 \tag{2.1}$$

where

$\tau(x_1,y_1)$: the intensity of a doublet located on the wing or in the wake (x_1,y_1);

S: wing surface;

W: wake.

$$r=\sqrt{(x-x_1)^2+(y-y_1)^2+z^2} \tag{2.2}$$

The intensity τ of a doublet is related to the potential at the discontinuity

$$\tau(x_1,y_1)=\phi(x_1,y_1,-0)-\phi(x_1,y_1,+0) \tag{2.3}$$

Using the following equaitons representing the pressure difference above and below the wing,

$$l(x_1,y_1)=c_{PL}(x_1,y_1)-c_{PU}(x_1,y_1)$$

c_{PU}: pressure coefficient above the wing (2.4)

c_{PL}: pressure coefficient below the wing

and the equation which is well known in the linear theory

$$c_P=-2\frac{1}{V}\frac{\partial\phi}{\partial x} \tag{2.5}$$

we obtain the following equation by rewriting (1.2), noting the fact that no pressure discontinuity exists in the wake (Ref. 4).

$$\phi(x,y,z)=\frac{Vz}{8\pi}\iint_S\frac{l(x_1,y_1)}{(y-y_1)^2+z^2}\left\{1+\frac{x-x_1}{\sqrt{(x-x_1)^2+(y-y_1)^2+z^2}}\right\}dx_1dy_1 \tag{2.6}$$

A downward flow v_z from this wing is derived by differentiating ϕ with respect to z, then the camber distribution z_c is determined from the following equation /5

$$\frac{\partial z_c}{\partial x}=\frac{v_z}{V}=\frac{1}{V}\frac{\partial\phi}{\partial z} \tag{2.7}$$

By means of (2.6) and (2.7), a camber distribution z_c which possesses the given load distribution $l(x,y)$ can be computed.

3. Outline of the Wing

The outline of the proposed wing consists of straight lines both at the leading and trailing edges, as shown in Figure 1. Let the sweep-back angle of the leading edge be φ and that of the trailing edge be ψ. Then the equations describing the leading edge line and the trailing edge line are, respectively, given as follows:

leading edge line $x_l-|y|\tan\varphi=0$ (3.1)

trailing edge line $x_t-1-|y|\tan\psi=0$ (3.2)

where the length is normalized by the wing-base chord length (OA of Figure 1).

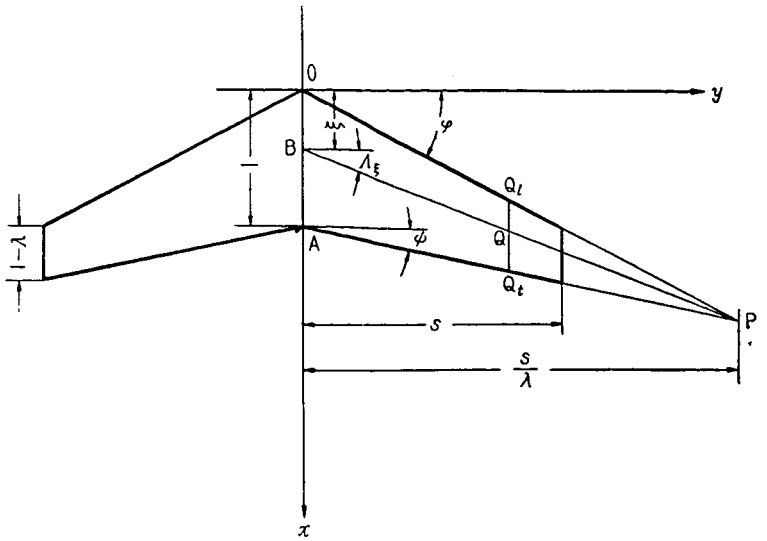

Figure 1. Outline of Wing

4. Load Distribution $l(x,y)$

The following two cases of load distribution are considered:

$$l_{1a}(x,y)=1(\xi-a)-1(\xi-1) \tag{4.1}$$

$$l_{2b}(x,y)=(\xi-b)[1(\xi-b)-1(\xi-1)] \tag{4.2}$$

where

$$\xi=\frac{x-|y|\tan\varphi}{1-\sigma|y|} \tag{4.3}$$

/6

$$\sigma=\frac{\lambda}{s} \tag{4.4}$$

$$1(x)=\begin{cases}1 : x\geqq 0\\ 0 : x<0\end{cases} \tag{4.5}$$

The geometrical meaning of ξ is as shown in Figure 1. The equation of the straight line which passes through the point B at a distance ξ from the leading edge along the chord at the wing base and the intersection P of the leading edge line and the trailing edge line is given by the following, letting the sweep-back angle of BP be Λ_ξ,

$$x-\xi=|y|\tan\Lambda_\xi \tag{4.6}$$

Using the following equation

$$\tan\varphi-\tan\Lambda_\xi=\frac{\lambda}{s}\xi \tag{4.7}$$

equation (4.6) can be rewritten in the following form

$$\xi=\frac{x-|y|\tan\varphi}{1-\sigma|y|} \tag{4.8}$$

At a point Q(x,y) on BP, the denominator at the right of the above equation is $\overline{Q_l Q_t}$ (local wing chord length) and the numerator is $\overline{Q_l Q}$ (the distance from the front edge to Q), when we let the intersections of a line parallel to the x-axis through Q with the leading-edge line and the trailing-edge line be Q_l and Q_t, respectively. (4.8) represents a trace of the point at which the ratio $\overline{Q_l Q}/\overline{Q_l Q_t}$ of the distance from the leading edge to that point and the local wing chord length passing through it is constant. In the case of the outline under consideration, consisting of straight lines both at the leading and trailing edges, this trace becomes a straight line passing through the point P. This trace is called the base line of the considered outline.

As may be observed from (4.1) and (4.2), the fact that $l(x,y)$ is a function of ξ alone indicates that the load distribution is constant along each base line. Namely, every base line on the wing surface becomes an isobar. Equations (4.1) and (4.2) are plotted in Figure 2.

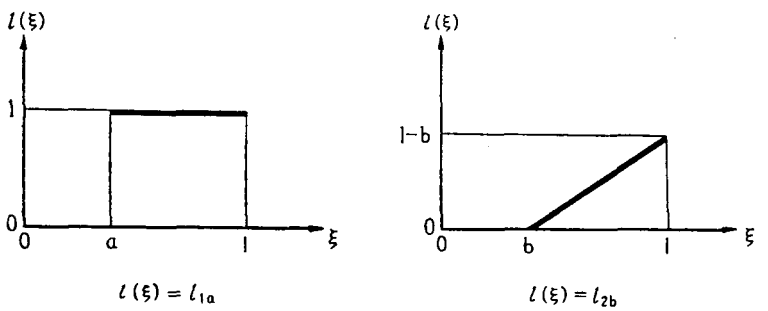

Figure 2. Load Distribution

If we analyze the load distributions given by (4.1) and (4.2) as a load distribution $l(x,y)$, all load distributions consisting of straight line segments can be represented by superimposing these two cases. For example, for the load distribution shown in Figure 3, it becomes /7

$$l(x,y)=Al_{1\alpha}-Bl_{1\beta}+\frac{B-A}{\beta-\alpha}(l_{2\alpha}-l_{2\beta})$$

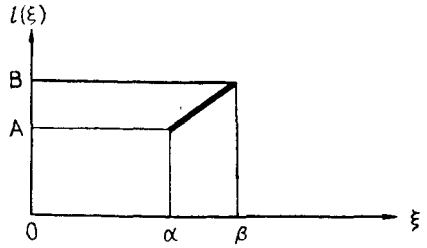

Figure 3. One Element of Tangential Load Distribution

5. Computational Method

When the load distribution $l(x_1,y_1)$ is a function of ξ_1 alone in (2.6), the integration with respect to y_1 can be carried out irrespective of $l(\xi_1)$, by converting the variable of integration from (x_1,y_1) to (ξ_1,y_1).

The result of the computations for

the outline of Figure 1 is given below. When the outline is symmetrical, the integration for the left wing ($y_1 < 0$) in (2.6) can be easily derived from that for the right wing ($y_1 > 0$). Hence, the computation was performed only for the right wing. This is indicated by r.

$$\phi_r(x,y,z)=\frac{V}{8\pi}\int_0^1 F(x,y,z,\xi_1)l(\xi_1)d\xi_1 \tag{5.1}$$

$$\begin{aligned}F(x,y,z,\xi_1)&=z\int_0^s \frac{1-\sigma y_1}{(y-y)^2+z^2}\left\{1+\frac{x-\xi_1-y_1\tan\Lambda_{\xi 1}}{\sqrt{(\xi_1-x+y_1\tan\Lambda_{\xi_1})^2+(y-y_1)^2+z^2}}\right\}dy_1\\
&=(1-\sigma y)\left\{\tan^{-1}\frac{s-y}{z}+\tan^{-1}\frac{y}{z}+\tan^{-1}\frac{[(s-y)^2+z^2]\tan\Lambda_{\xi_1}+x_{r\xi_1}(s-y)}{z\sqrt{x_r{}^2{}_{\xi_1}+(s-y)^2+z^2}}\right.\\
&\qquad\left.-\tan^{-1}\frac{(y^2+z^2)\tan\Lambda_{\xi_1}+y(\xi_1-x)}{z\sqrt{(x-\xi_1)^2+y^2+z^2}}\right\}\\
&\quad+\sigma z\log\left\{\frac{\sqrt{(x-\xi_1)^2+y^2+z^2}-(x-\xi_1)}{\sqrt{x_r{}^2{}_{\xi_1}+(s-y)^2+z^2}-x_{r\xi_1}}\right\}\\
&\quad+\sigma z\sin\Lambda_{\xi_1}\log\left\{\frac{\sqrt{x_r{}^2{}_{\xi_1}+(s-y)^2+z^2}+s\sec\Lambda_{\xi_1}-(x-\xi_1)\sin\Lambda_{\xi_1}-y\cos\Lambda_{\xi_1}}{\sqrt{(x-\xi_1)^2+y^2+z^2}-(x-\xi_1)\sin\Lambda_{\xi_1}-y\cos\Lambda_{\xi_1}}\right\}\end{aligned} \tag{5.2}$$

where /8

$$\tan\Lambda_{\xi_1}=\tan\varphi-\frac{\lambda}{s}\xi_1 \tag{5.3}$$

$$x_{r\xi_1}=x-\xi_1-s\tan\Lambda_{\xi_1} \tag{5.4}$$

As for the portion ϕ_l arising from the integration of the left wing, it can be immediately obtained from ϕ_r using the relationship

$$\phi_l(x,y,z)=\phi_r(x,-y,z) \tag{5.5}$$

Finally it becomes

$$\phi=\phi_r+\phi_l=\phi_r(x,y,z)+\phi_r(x,-y,z) \tag{5.6}$$

The representation of (5.1) may be useful as a fundamental equation for numerical computations when the form of $l(\xi_1)$ is complex, and the analytical solution of the double integration in (2.6) is impossible. However, when the load distribution $l(\xi_1)$ possesses a simple form such as (4.1) and (4.2), it is easier to integrate over y_1 after having integrated over ξ_1 in (2.6).

When z_c is obtained from the given $l(\xi_1)$ by means of (2.7), using (2.6) as a fundamental equation, it is sufficient to find v_z in order to derive the camber distribution z_c. Therefore, the computation may be simplified by carrying out the differentiation of ϕ with respect to z in (2.7) before the integration.

6. Results of Computations

The results of the computation, which was performed to obtain the downward flow v_z of a thin wing having the load distributions $l_1(\xi)$ and $l_2(\xi)$ stated in (Ref. 4) for the outline of (Ref. 3), are given below. In this case, (2.6)

is described as follows:

$$\phi_r=\frac{Vz}{8\pi}\int_0^1\frac{1-\sigma y_1}{(y-y_1)^2+z^2}dy_1\int_0^1 l(\xi_1)\left\{1+\frac{x-x_1}{\sqrt{(x-x_1)^2+(y-y_1)^2+z^2}}\right\}d\xi_1 \tag{6.1}$$

$$x_1=(1-\sigma|y_1|)\xi_1+|y_1|\tan\varphi \tag{6.2}$$

Let ϕ and v_z for the given $l_1(\xi_1)$ by (4.1) be ϕ_1 and v_{z1}, respectively, and let those for $l_2(\xi_1)$ given by (4.2) be ϕ_2 and v_{z2}.

6.1 $l_{1a}(\xi_1)=1(\xi_1-a)-1(\xi_1-1)$

$$\begin{aligned}\phi_{r1}\Big/\left(\frac{Vz}{8\pi}\right)=&(1-a)\left\{\frac{1-\sigma y}{z}\left(\tan^{-1}\frac{s-y}{z}+\tan^{-1}\frac{y}{z}\right)+\frac{\sigma}{2}\log\left[\frac{y^2+z^2}{(s-y)^2+z^2}\right]\right\}\\&+\sec\chi\log\left\{\frac{\sqrt{x_{ra}^2+(s-y)^2+z^2}+s\sec\chi-(x-a)\sin\chi-y\cos\chi}{\sqrt{(x-a)^2+y^2+z^2}-(x-a)\sin\chi-y\cos\chi}\right\}\\&-\frac{\tan\chi}{2}\log\left\{\frac{\sqrt{x_{ra}^2+(s-y)^2+z^2}-x_{ra}}{\sqrt{x_{ra}^2+(s-y)^2+z^2}+x_{ra}}\cdot\frac{\sqrt{(x-a)^2+y^2+z^2}+x-a}{\sqrt{(x-a)^2+y^2+z^2}-(x-a)}\right\}\\&+\frac{x-a-y\tan\chi}{z}\left\{\tan^{-1}\frac{[(s-y)^2+z^2]\tan\chi+x_{ra}(s-y)}{z\sqrt{x_{ra}^2+(s-y)^2+z^2}}\right.\\&\qquad\left.-\tan^{-1}\frac{(y^2+z^2)\tan\chi-(x-a)y}{z\sqrt{(x-a)^2+y^2+z^2}}\right\}\\&-\sec\psi\log\left\{\frac{\sqrt{x_{r1}^2+(s-y)^2+z^2}+s\sec\psi-(x-1)\sin\psi-y\cos\psi}{\sqrt{(x-1)^2+y^2+z^2}-(x-1)\sin\psi-y\cos\psi}\right\}\\&+\frac{\tan\psi}{2}\log\left\{\frac{\sqrt{x_{r1}^2+(s-y)^2+z^2}-x_{r1}}{\sqrt{x_{r1}^2+(s-y)^2+z^2}+x_{r1}}\cdot\frac{\sqrt{(x-1)^2+y^2+z^2}+x-1}{\sqrt{(x-1)^2+y^2+z^2}-(x-1)}\right\}\\&-\frac{x-1-y\tan\psi}{z}\left\{\tan^{-1}\frac{[(s-y)^2+z^2]\tan\psi+x_{r1}(s-y)}{z\sqrt{x_{r1}^2+(s-y)^2+z^2}}\right.\\&\qquad\left.-\tan^{-1}\frac{(y^2+z^2)\tan\psi-(x-1)y}{z\sqrt{(x-1)^2+y^2+z^2}}\right\}\end{aligned} \tag{6.3}$$

where /9

$$x_{ra}=x-a-s\tan\chi \tag{6.4}$$

$$x_{r1}=x-1-s\tan\psi \tag{6.5}$$

$$\tan\chi=\tan\varphi-(\lambda/s)a \tag{6.6}$$

$$\begin{aligned}8\pi\left(\frac{v_{zr1}}{V}\right)=&(1-a)\left\{\frac{\sigma}{2}\log\left[\frac{y^2+z^2}{(s-y)^2+z^2}\right]-\frac{y}{y^2+z^2}+(\lambda-1)\frac{s-y}{(s-y)^2+z^2}\right\}\\&+\sec\chi\log\left\{\frac{\sqrt{x_{ra}^2+(s-y)^2+z^2}+s\sec\chi-(x-a)\sin\chi-y\cos\chi}{\sqrt{(x-a)^2+y^2+z^2}-(x-a)\sin\chi-y\cos\chi}\right\}\\&-\frac{\tan\chi}{2}\log\left\{\frac{\sqrt{x_{ra}^2+(s-y)^2+z^2}-x_{ra}}{\sqrt{x_{ra}^2+(s-y)^2+z^2}+x_{ra}}\cdot\frac{\sqrt{(x-a)^2+y^2+z^2}+x-a}{\sqrt{(x-a)^2+y^2+z^2}-(x-a)}\right\}\\&-\frac{(s-y)\sqrt{x_{ra}^2+(s-y)^2+z^2}}{(s-y)^2+z^2}-\frac{y\sqrt{(x-a)^2+y^2+z^2}}{y^2+z^2}\\&-\sec\psi\log\left\{\frac{\sqrt{x_{r1}^2+(s-y)^2+z^2}+s\sec\psi-(x-1)\sin\psi-y\cos\psi}{\sqrt{(x-1)^2+y^2+z^2}-(x-1)\sin\psi-y\cos\psi}\right\}\end{aligned} \tag{6.7}$$

$$+\frac{\tan\psi}{2}\log\left\{\frac{\sqrt{x_{r1}^2+(s-y)^2+z^2}-x_{r1}}{\sqrt{x_{r1}^2+(s-y)^2+z^2}+x_{r1}}\cdot\frac{\sqrt{(x-1)^2+y^2+z^2}+x-1}{\sqrt{(x-1)^2+y^2+z^2}-(x-1)}\right\} \tag{6.7}$$

$$+\frac{(s-y)\sqrt{x_{r1}^2+(s-y)^2+z^2}}{(s-y)^2+z^2}+\frac{y\sqrt{(x-1)^2+y^2+z^2}}{y^2+z^2}$$

In the above v_{zr1}, we observe that the 5th term $-y\sqrt{(x-a)^2+y^2+z^2}/(y^2+z^2)$ and the last term $y\sqrt{(x-1)^2+y^2+z^2}/(y^2+z^2)$ do not contribute to v_{z1} from the relation of (5.6).

6.2 $l_{2b}(\xi_1)=(\xi_1-b)[1(\xi_1-b)-1(\xi_1-1)]$

$$\rho=\frac{s}{\lambda}=\frac{1}{\sigma}$$

Let /10

$$\phi_{r2}\Big/\left(\frac{Vz}{8\pi}\right)=\frac{1}{2}(1-b)^2K_1-(1-b)K_2+\frac{\rho}{2}(K_3+K_4)$$

$$K_1=\frac{1-\sigma y}{z}\left(\tan^{-1}\frac{s-y}{z}+\tan^{-1}\frac{y}{z}\right)+\frac{\sigma}{2}\log\left\{\frac{y^2+z^2}{(s-y)^2+z^2}\right\}$$

$$K_2=\sec\psi\log\left\{\frac{\sqrt{x_{r1}^2+(s-y)^2+z^2}+s\sec\psi-(x-1)\sin\psi-y\cos\psi}{\sqrt{(x-1)^2+y^2+z^2}-(x-1)\sin\psi-y\cos\psi}\right\}$$

$$-\frac{\tan\psi}{2}\log\left\{\frac{\sqrt{x_{r1}^2+(s-y)^2+z^2}-x_{r1}}{\sqrt{x_{r1}^2+(s-y)^2+z^2}+x_{r1}}\cdot\frac{\sqrt{(x-1)^2+y^2+z^2}+x-1}{\sqrt{(x-1)^2+y^2+z^2}-(x-1)}\right\}$$

$$+\frac{x-1-y\tan\psi}{z}\left\{\tan^{-1}\frac{[(s-y)^2+z^2]\tan\psi+x_{r1}(s-y)}{z\sqrt{(x_{r1}^2+(s-y)^2+z^2}}\right.$$

$$\left.-\tan^{-1}\frac{(y^2+z^2)\tan\psi-(x-1)y}{z\sqrt{(x-1)^2+y^2+z^2}}\right\}$$

$$K_3=\sec\Omega\tan\Omega\log\left\{\frac{\sqrt{x_{rb}^2+(s-y)^2+z^2}+s\sec\Omega-(x-b)\sin\Omega-y\cos\Omega}{\sqrt{(x-b)^2+y^2+z^2}-(x-b)\sin\Omega-y\cos\Omega}\right\} \tag{6.8}$$

$$-\frac{(x-\rho\tan\varphi)\sqrt{(x-\rho\tan\varphi)^2+(y-\rho)^2+z^2}}{(y-\rho)^2+z^2}$$

$$\times\left\{\log\left|\frac{\sqrt{x_{rb}^2+(s-y)^2+z^2}-\sqrt{(x-\rho\tan\varphi)^2+(y-\rho)^2+z^2}+(s-\rho)\sec\Omega}{\sqrt{x_{rb}^2+(s-y)^2+z^2}+\sqrt{(x-\rho\tan\varphi)^2+(y-\rho)^2+z^2}+(s-\rho)\sec\Omega}\right|\right.$$

$$\left.-\log\left|\frac{\sqrt{(x-b)^2+y^2+z^2}-\sqrt{(x-\rho\tan\varphi)^2+(y-\rho)^2+z^2}-\rho\sec\Omega}{\sqrt{(x-b)^2+y^2+z^2}+\sqrt{(x-\rho\tan\varphi)^2+(y-\rho)^2+z^2}-\rho\sec\Omega}\right|\right\}$$

$$+\frac{1}{2}\left\{\frac{(x-\rho\tan\varphi)^2}{(y-\rho)^2+z^2}-\tan^2\Omega\right\}$$

$$\times\log\left\{\frac{\sqrt{x_{rb}^2+(s-y)^2+z^2}-x_{rb}}{\sqrt{x_{rb}^2+(s-y)^2+z^2}+x_{rb}}\cdot\frac{\sqrt{(x-b)^2+y^2+z^2}+x-b}{\sqrt{(x-b)^2+y^2+z^2}-(x-b)}\right\}$$

$$-\frac{(x-b-y\tan\Omega)^2(y-\rho)-z^2\tan\Omega[2(x-b)-(y+\rho)\tan\Omega]}{z[(y-\rho)^2+z^2]}$$

$$\times\left\{\tan^{-1}\frac{[(s-y)^2+z^2]\tan\Omega+x_{rb}(s-y)}{\sqrt{x_{rb}^2+(s-y)^2+z^2}}-\tan^{-1}\frac{(y^2+z^2)\tan\Omega-(x-b)y}{\sqrt{(x-b)^2+y^2+z^2}}\right\}$$

$$
\begin{aligned}
&-\sec\psi\tan\psi\log\left\{\frac{\sqrt{x_{r1}^2+(s-y)^2+z^2}+s\sec\psi-(x-1)\sin\psi-y\cos\psi}{\sqrt{(x-1)^2+y^2+z^2}-(x-1)\sin\psi-y\cos\psi}\right\}\\
&+\frac{(x-\rho\tan\varphi)\sqrt{(x-\rho\tan\varphi)^2+(y-\rho)^2+z^2}}{(y-\rho)^2+z^2}\\
&\times\left\{\log\left|\frac{\sqrt{x_{r1}^2+(s-y)^2+z^2}-\sqrt{(x-\rho\tan\varphi)^2+(y-\rho)^2+z^2}+(s-\rho)\sec\psi}{\sqrt{x_{r1}^2+(s-y)^2+z^2}+\sqrt{(x-\rho\tan\varphi)^2+(y-\rho)^2+z^2}+(s-\rho)\sec\psi}\right|\right.\\
&\left.-\log\left|\frac{\sqrt{(x-1)^2+y^2+z^2}-\sqrt{(x-\rho\tan\varphi)^2+(y-\rho)^2+z^2}-\rho\sec\psi}{\sqrt{(x-1)^2+y^2+z^2}+\sqrt{(x-\rho\tan\varphi)^2+(y-\rho)^2+z^2}-\rho\sec\psi}\right|\right\}\\
&-\frac{1}{2}\left\{\frac{(x-\rho\tan\varphi)^2}{(y-\rho)^2+z^2}-\tan^2\psi\right\}\\
&\times\log\left\{\frac{\sqrt{x_{r1}^2+(s-y)^2+z^2}-x_{r1}}{\sqrt{x_{r1}^2+(s-y)^2+z^2}+x_{r1}}\cdot\frac{\sqrt{(x-1)^2+y^2+z^2}+x-1}{\sqrt{(x-1)^2+y^2+z^2}-(x-1)}\right\}\\
&+\frac{(x-1-y\tan\psi)^2(y-\rho)-z^2\tan\psi[2(x-1)-(y+\rho)\tan\psi]}{z[(y-\rho)^2+z^2]}\\
&\times\left\{\tan^{-1}\frac{[(s-y)^2+z^2]\tan\psi+x_{r1}(s-y)}{z\sqrt{x_{r1}^2+(s-y)^2+z^2}}-\tan^{-1}\frac{(y^2+z^2)\tan\psi-(x-1)y}{z\sqrt{(x-1)^2+y^2+z^2}}\right\}
\end{aligned}
\tag{6.8}
$$

$$
K_4=\int_0^s\frac{1}{\rho-y_1}\log\left\{\frac{\sqrt{(x-1-y_1\tan\psi)^2+(y-y_1)+z^2}-(x-1-y_1\tan\psi)}{\sqrt{(x-b-y_1\tan\Omega)^2+(y-y_1)^2+z^2}-(x-b-y_1\tan\Omega)}\right\}dy_1
$$

where

$$
x_{rb}=x-b-s\tan\Omega
$$

$$
\tan\Omega=\tan\varphi-(\lambda/s)b
$$

/11

Since the integration of K_4 could be represented by elementary functions, it was numerically integrated in the actual computation.

$$
\begin{aligned}
8\pi\left(\frac{v_{zr2}}{V}\right)&=\frac{1}{2}(1-b)^2J_1-(1-b)J_2+\frac{\rho}{2}(J_3+J_4+J_5)\\
J_1&=\frac{\sigma}{2}\log\left\{\frac{y^2+z^2}{(s-y)^2+z^2}\right\}-\frac{y}{y^2+z^2}+(\lambda-1)\frac{s-y}{(s-y)^2+z^2}\\
J_2&=\sec\psi\log\left\{\frac{\sqrt{x_{r1}^2+(s-y)^2+z^2}+s\sec\psi-(x-1)\sin\psi-y\cos\psi}{\sqrt{(x-1)^2+y^2+z^2}-(x-1)\sin\psi-y\cos\psi}\right\}\\
&\quad-\frac{\tan\psi}{2}\log\left\{\frac{\sqrt{x_{r1}^2+(s-y)^2+z^2}-x_{r1}}{\sqrt{x_{r1}^2+(s-y)^2+z^2}+x_{r1}}\cdot\frac{\sqrt{(x-1)^2+y^2+z^2}+x-1}{\sqrt{(x-1)^2+y^2+z^2}-(x-1)}\right\}\\
&\quad-\frac{(s-y)\sqrt{x_{r1}^2+(s-y)^2+z^2}}{(s-y)^2+z^2}-\frac{y\sqrt{(x-1)^2+y^2+z^2}}{y^2+z^2}\\
J_3&=\sec\Omega\tan\Omega\log\left\{\frac{\sqrt{x_{rb}^2+(s-y)^2+z^2}+s\sec\Omega-(x-b)\tan\Omega-y\cos\Omega}{\sqrt{(x-b)^2+y^2+z^2}-(x-b)\sin\Omega-y\cos\Omega}\right\}\\
&\quad-\frac{(x-\rho\tan\varphi)\{(y-\rho)^2[(x-\rho\tan\varphi)^2+(y-\rho)^2]+z^2[(y-\rho)^2-(x-\rho\tan\varphi)^2]\}}{[(y-\rho)^2+z^2]^2\sqrt{(x-\rho\tan\varphi)^2+(y-\rho)^2+z^2}}\\
&\quad\times\left\{\log\left|\frac{\sqrt{x_{rb}^2+(s-y)^2+z^2}-\sqrt{(x-\rho\tan\varphi)^2+(y-\rho)^2+z^2}+(s-\rho)\sec\Omega}{\sqrt{x_{rb}^2+(s-y)^2+z^2}+\sqrt{(x-\rho\tan\varphi)^2+(y-\rho)^2+z^2}+(s-\rho)\sec\Omega}\right|\right.\\
&\quad\left.-\log\left|\frac{\sqrt{(x-b)^2+y^2+z^2}-\sqrt{(x-\rho\tan\varphi)^2+(y-\rho)^2+z^2}-\rho\sec\Omega}{\sqrt{(x-b)^2+y^2+z^2}+\sqrt{(x-\rho\tan\varphi)^2+(y-\rho)^2+z^2}+\rho\sec\Omega}\right|\right\}
\end{aligned}
\tag{6.9}
$$

$$+\frac{1}{2}\left\{\frac{(x-\rho\tan\varphi)^2[(y-\rho)^2-z^2]}{[(y-\rho)^2+z^2]^2}-\tan^2\Omega\right\}$$

$$\times\log\left\{\frac{\sqrt{x_{rb}^2+(s-y)^2+z^2}-x_{rb}}{\sqrt{x_{rb}^2+(s-y)^2+z^2}+x_{rb}}\cdot\frac{\sqrt{(x-b)^2+y^2+z^2}+x-b}{\sqrt{(x-b)^2+y^2+z^2}-(x-b)}\right\}$$

$$+\frac{2z(x-\rho\tan\varphi)^2(y-\rho)}{[(y-\rho)^2+z^2]^2}$$

$$\times\left\{\tan^{-1}\frac{[(s-y)^2+z^2]\tan\Omega+x_{rb}(s-y)}{z\sqrt{x_{rb}^2+(s-y)^2+z^2}}-\tan^{-1}\frac{(y^2+z^2)\tan\Omega-(x-b)y}{z\sqrt{(x-b)^2+y^2+z^2}}\right\}$$

$$-\frac{(x-b-y\tan\Omega)(\rho-y)(s-y)+[(\rho-y)\tan\Omega-x_{rb}]z^2}{[(s-y)^2+z^2][(\rho-y)^2+z^2]}\sqrt{x_{rb}^2+(s-y)^2+z^2}$$

$$+\frac{(x-b-y\tan\Omega)(y-\rho)y+[(\rho-y)\tan\Omega-(x-b)]z^2}{(y^2+z^2)[(\rho-y)^2+z^2]}\sqrt{(x-b)^2+y^2+z^2}$$

$$+\frac{z^2(x-\rho\tan\varphi)}{(y-\rho)^2+z^2}\left\{\frac{1}{\sqrt{x_{rb}^2+(s-y)^2+z^2}}-\frac{1}{\sqrt{(x-b)^2+y^2+z^2}}\right\}$$

$$-\sec\psi\tan\psi\log\left\{\frac{\sqrt{x_{r1}^2+(s-y)^2+z^2}+s\sec\psi-(x-1)\sin\psi-y\cos\psi}{\sqrt{(x-1)^2+y^2+z^2}-(x-1)\sin\psi-y\cos\psi}\right\}$$

$$+\frac{(x-\rho\tan\varphi)\{(y-\rho)^2[(x-\rho\tan\varphi)^2+(y-\rho)^2]+z^2[(y-\rho)^2-(x-\rho\tan\varphi)^2]\}}{[(y-\rho)^2+z^2]^2\sqrt{(x-\rho\tan\varphi)^2+(y-\rho)^2+z^2}}$$

$$\times\left\{\log\left|\frac{\sqrt{x_{r1}^2+(s-y)^2+z^2}-\sqrt{(x-\rho\tan\varphi)^2+(y-\rho)^2+z^2}+(s-\rho)\sec\psi}{\sqrt{x_{r1}^2+(s-y)^2+z^2}+\sqrt{(x-\rho\tan\varphi)^2+(y-\rho)^2+z^2}+(s-\rho)\sec\psi}\right|\right.$$

$$\left.-\log\left|\frac{\sqrt{(x-1)^2+y^2+z^2}-\sqrt{(x-\rho\tan\varphi)^2+(y-\rho)^2+z^2}-\rho\sec\psi}{\sqrt{(x-1)^2+y^2+z^2}+\sqrt{(x-\rho\tan\varphi)^2+(y-\rho)^2+z^2}-\rho\sec\psi}\right|\right\} \qquad (6.9)$$

$$-\frac{1}{2}\left\{\frac{(x-\rho\tan\varphi)^2[(y-\rho)^2-z^2]}{[(y-\rho)^2+z^2]^2}-\tan^2\psi\right\}$$

$$\times\log\left\{\frac{\sqrt{x_{r1}^2+(s-y)^2+z^2}-x_{r1}}{\sqrt{x_{r1}^2+(s-y)^2+z^2}+x_{r1}}\cdot\frac{\sqrt{(x-1)^2+y^2+z^2}+x-1}{\sqrt{(x-1)^2+y^2+z^2}-(x-1)}\right\}$$

$$-\frac{2z(y-\rho)(x-\rho\tan\varphi)^2}{[(y-\rho)^2+z^2]^2}$$

$$\times\left\{\tan^{-1}\frac{[(s-y)^2+z^2]\tan\psi+x_{r1}(s-y)}{z\sqrt{x_{r1}^2+(s-y)^2+z^2}}-\tan^{-1}\frac{(y^2+z^2)\tan\psi-(x-1)y}{z\sqrt{(x-1)^2+y^2+z^2}}\right\}$$

$$+\frac{(x-1-y\tan\psi)(\rho-y)(s-y)+[(\rho-y)\tan\psi-x_{r1}]z^2}{[(s-y)^2+z^2][(\rho-y)^2+z^2]}\sqrt{x_{r1}^2+(s-y)^2+z^2}$$

$$-\frac{(x-1-y\tan\psi)\,y\,(y-\rho)+[(\rho-y)\tan\psi-(x-1)]z^2}{(y^2+z^2)[(\rho-y)^2+z^2]}\sqrt{(x-1)^2+y^2+z^2}$$

$$-\frac{z^2(x-\rho\tan\varphi)}{(y-\rho)^2+z^2}\left\{\frac{1}{\sqrt{x_{r1}^2+(s-y)^2+z^2}}-\frac{1}{\sqrt{(x-1)^2+y^2+z^2}}\right\}$$

$$J_4=\frac{(x-\rho\tan\varphi)z^2}{[(\rho-y)^2+z^2]\sqrt{(x-\rho\tan\varphi)^2+(\rho-y)^2+z^2}}$$

$$\times\left\{\log\left|\frac{\sqrt{x_{rb}^2+(s-y)^2+z^2}-\sqrt{(x-\rho\tan\varphi)^2+(\rho-y)^2+z^2}+(s-\rho)\sec\Omega}{\sqrt{x_{rb}^2+(s-y)^2+z^2}+\sqrt{(x-\rho\tan\varphi)^2+(\rho-y)^2+z^2}+(s-\rho)\sec\Omega}\right|\right.$$

$$\left.-\log\left|\frac{\sqrt{(x-b)^2+y^2+z^2}-\sqrt{(x-\rho\tan\varphi)^2+(\rho-y)^2+z^2}-\rho\sec\Omega}{\sqrt{(x-b)^2+y^2+z^2}+\sqrt{(x-\rho\tan\varphi)^2+(\rho-y)^2+z^2}-\rho\sec\Omega}\right|\right\}$$

$$+\frac{z^2}{2[(\rho-y)^2+z^2]}\log\left\{\frac{\sqrt{x_{rb}^2+(s-y)^2+z^2}+x_{rb}}{\sqrt{x_{rb}^2+(s-y)^2+z^2}-x_{rb}}\cdot\frac{\sqrt{(x-b)^2+y^2+z^2}-(x-b)}{\sqrt{(x-b)^2+y^2+z^2}+x-b}\right\}$$

$$+\frac{z(y-\rho)}{(\rho-y)^2+z^2}\left\{\tan^{-1}\frac{[(s-y)^2+z^2]\tan\Omega+x_{rb}(s-y)}{z\sqrt{x_{rb}^2+(s-y)^2+z^2}}\right.$$

$$\left.-\tan^{-1}\frac{(y^2+z^2)\tan\Omega-(x-b)y}{z\sqrt{(x-b)^2+y^2+z^2}}\right\}$$

$$-\frac{(x-\rho\tan\varphi)z^2}{[(\rho-y)^2+z^2]\sqrt{(x-\rho\tan\varphi)^2+(\rho-y)^2+z^2}}$$

$$\times\left\{\log\left|\frac{\sqrt{x_{r1}^2+(s-y)^2+z^2}-\sqrt{(x-\rho\tan\varphi)^2+(\rho-y)^2+z^2}+(s-\rho)\sec\psi}{\sqrt{x_{r1}^2+(s-y)^2+z^2}+\sqrt{(x-\rho\tan\varphi)^2+(\rho-y)^2+z^2}+(s-\rho)\sec\psi}\right|\right.$$

$$\left.-\log\left|\frac{\sqrt{(x-1)^2+y^2+z^2}-\sqrt{(x-\rho\tan\varphi)^2+(\rho-y)^2+z^2}-\rho\sec\psi}{\sqrt{(x-1)^2+y^2+z^2}+\sqrt{(x-\rho\tan\varphi)^2+(\rho-y)^2+z^2}-\rho\sec\psi}\right|\right\} \qquad (6.9)\ /13$$

$$-\frac{z^2}{2[(\rho-y)^2+z^2]}\log\left\{\frac{\sqrt{x_{r1}^2+(s-y)^2+z^2}+x_{r1}}{\sqrt{x_{r1}^2+(s-y)^2+z^2}-x_{r1}}\cdot\frac{\sqrt{(x-1)^2+y^2+z^2}-(x-1)}{\sqrt{(x-1)^2+y^2+z^2}+x-1}\right\}$$

$$-\frac{z(y-\rho)}{(\rho-y)^2+z^2}\left\{\tan^{-1}\frac{[(s-y)^2+z^2]\tan\psi+x_{r1}(s-y)}{z\sqrt{x_{r1}^2+(s-y)^2+z^2}}\right.$$

$$\left.-\tan^{-1}\frac{(y^2+z^2)\tan\psi-(x-1)y}{z\sqrt{(x-1)^2+y^2+z^2}}\right\}$$

$$J_5=\int_0^s\frac{1}{\rho-y_1}\log\left\{\frac{\sqrt{(x-1-y_1\tan\psi)^2+(y-y_1)^2+z^2}-(x-1-y_1\tan\psi)}{\sqrt{(x-b-y_1\tan\Omega)^2+(y-y_1)^2+z^2}-(x-b-y_1\tan\Omega)}\right\}dy_1$$

The velocity disturbance v_z in the z-direction is given as above. Then the camber distribution z_c is computed from (2.7) using it. It is sufficient to know v_z alone in order to obtain the camber distribution z_c. However, it becomes necessary to know the disturbance velocities v_x and v_y in the x- and y-directions when details of the flow field are desired, and they are obtained by differentiating the disturbance potential ϕ in each direction. These computational results are given in the appendix.

7. Shape of the Camber

The fundamental equation (2.1) is the representation of the case when the considered wing surface is assumed to lie in the plane z = 0. Accordingly, z_c is computed after having obtained v_z at z = 0 in (2.7), and this is the standpoint of the ordinary linear theory.

However, z = 0 becomes a singularity of v_z at the center y = 0 and tip y = = s of the wing, as observed from the expression of v_z in [6], so that z_c cannot be computed. In order to avoid this, Weber obtained v_z at $z = z_t$, taking into account the thickness z_t of the wing, and then computed z_c (Ref. 4).

Following Weber's procedure, we computed z_b from the descending flow v_z at $z = z_t$.

$$z_c(x, y)=\int_{x_l}^{x} \frac{v_z(x, y, z_l)}{V} dx \tag{7.1}$$

In the numerical example [9] presented below, we used NACA 64A 010 as z_t, modifying it (Ref. 6) according to Küchemann's method (Ref. 3). /14

This z_c is separated into the local elevation angle $\alpha(y)$ and the ordinary camber distribution z_{cm} as follows

$$\alpha(y)=-\tan^{-1}\frac{z_c(x_t, y)}{x_t-x_l} \tag{7.2}$$

$$z_{cm}(x, y)=z_c(x, y)+(x-x_l)\tan\alpha$$

$$=z_c(x, y)-\frac{x-x_l}{x_t-x_l}z_c(x_t, y) \tag{7.3}$$

Examples of computation of $\alpha(y)$ and $z_{cm}(x,y)$ are presented in [9].

8. Vertical Distribution of Mach Numbers

As stated in [1], the greatest effect of the sweep-back angle is the reduction in the normal component of Mach numbers M_n at the isobars. Therefore, it is interesting to know how M_n is distributed on the wing surface which possesses the camber distribution computed by the preceding method (Ref. 5).

Assume that the wing surface is at z = 0 and draw an isobar line on it. Let the angle between the isobar and the y-axis (the direction normal to the main stream on the wing surface) at a point P be Λ, then the velocity V_n which is normal to the isobar at that point is given by the following equation

$$V_n^2=\{(V+v_x)\cos\Lambda-v_y\sin\Lambda\}^2+v_z^2 \tag{8.1}$$

Using this, we can obtain a representation of M_n within the approximation of the linear theory.

$$\left(\frac{M_n}{M_\infty}\right)^2=\left(\frac{M}{M_\infty}\right)^2\cos^2\Lambda-\left(\frac{v_y}{V}\right)\left(\frac{a_\infty}{a}\right)^2\sin 2\Lambda \tag{8.2}$$

where

M: Mach number at point P;
M_∞: Mach number of uniform flow;
a: Sonic speed at the point P;
a_∞: Sonic speed of uniform flow.

Namely, M_n can be obtained provided v_y/V and Λ are known.

In the subsequent section, an example of M_n distribution is presented together with z_c.

9. Numerical Example

Examples of numerical computation using the method stated in the previous sections are presented. Since the equations are for incompressible gas, the case of compressible gas is to be reduced to the incompressible case by means of the appropriate conversion. We used Prandtl-Glauert's law for this purpose. /15

Physical quantities in compressible flows are indicated below by a suffix c.

Mach number	$M_\infty = 0.8$
Wing outline	
Half wing-span	$s_c = 3.6$
Taper ratio	$1 - \lambda = 0.5$
Sweep-back angle of the leading edge	$\varphi_c = 30°$
Aspect ratio	$AR_c = 9/6$

According to Prandtl-Glauret's law, the aspect ratio in the corresponding incompressible flow is 5.8.

Load Distribution

As a load distribution, the following two cases are considered:

(i) $$l(\xi)=0.3\times l_1(\xi,0)$$

(ii) $$l(\xi)=0.4\times l_1(\xi,0)-0.8\times l_2(\xi,0.5)$$

where

$$l_1(\xi,a)=1(\xi-a)-1(\xi-1)$$

$$l_2(\xi,b)=(\xi-b)[1(\xi-b)-1(\xi-1)]$$

Both (i) and (ii) correspond to the lift coefficient $C_L = 0.3$.

Figure 4 shows a comparison of the spanwise distribution of the local elevation angle for the case of a semi-infinite-span wing (Ref. 6). In the neighborhood of the wing base, the elevation angle becomes larger than that of the semi-infinite-span wing.

Figure 5 gives a comparison of z_{cm} at various points in the span-wise direction. The variation of z_{cm} with respect to y is not monotonic.

Figure 6 (a) - (c) gives comparisons of z_{cm} with the case of a semi-infinite-span wing. The difference from the semi-infinite-span wing becomes conspicuous close to the wing base.

Figure 7 gives a variation of z_{cm} with s, and Figure 8 gives a variation

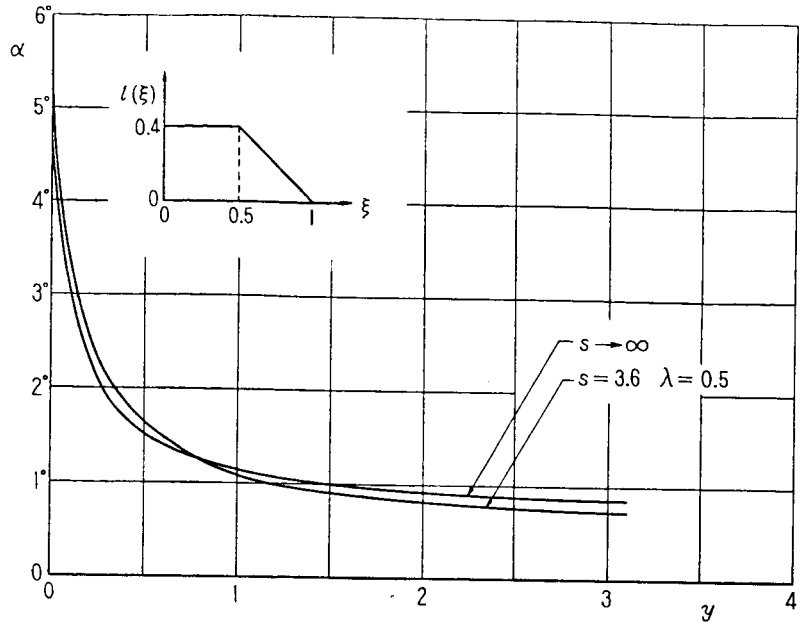

Figure 4. Variation of α with y.

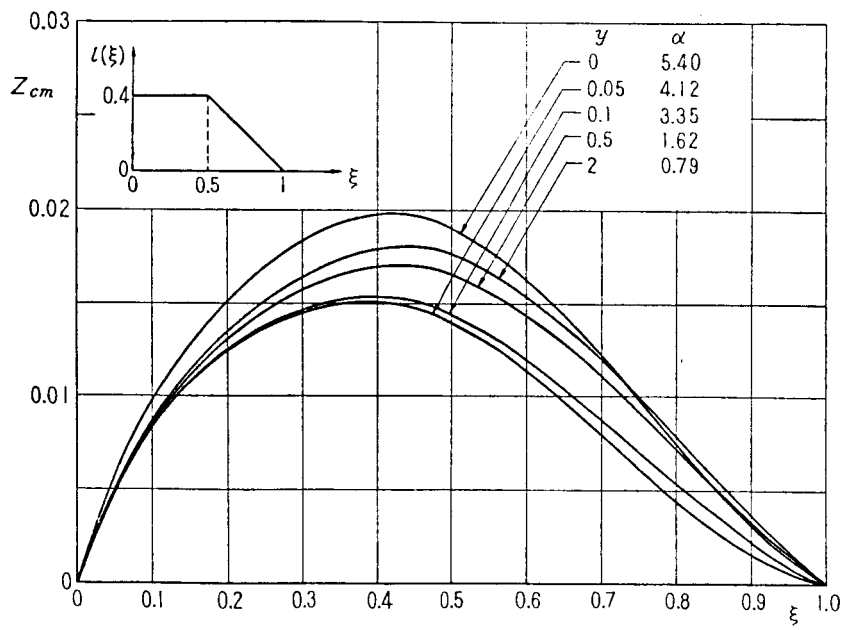

Figure 5. Variation of z_{cm} with y

with λ. Both variations are small, indicating that the effect of the aspect ratio is not remarkable.

On the other hand, the effect of the sweep-back angle is remarkable, as observed from Figure 9.

Figure 10 demonstrates the manner in which the shape of the load

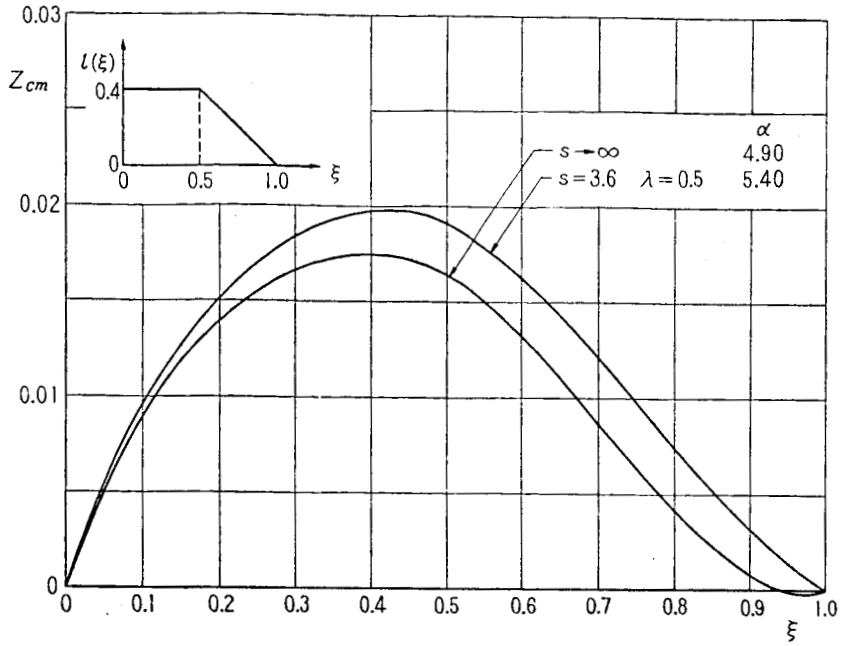

Figure 6 (a). Comparison of z_{cm} : y = 0.

/17

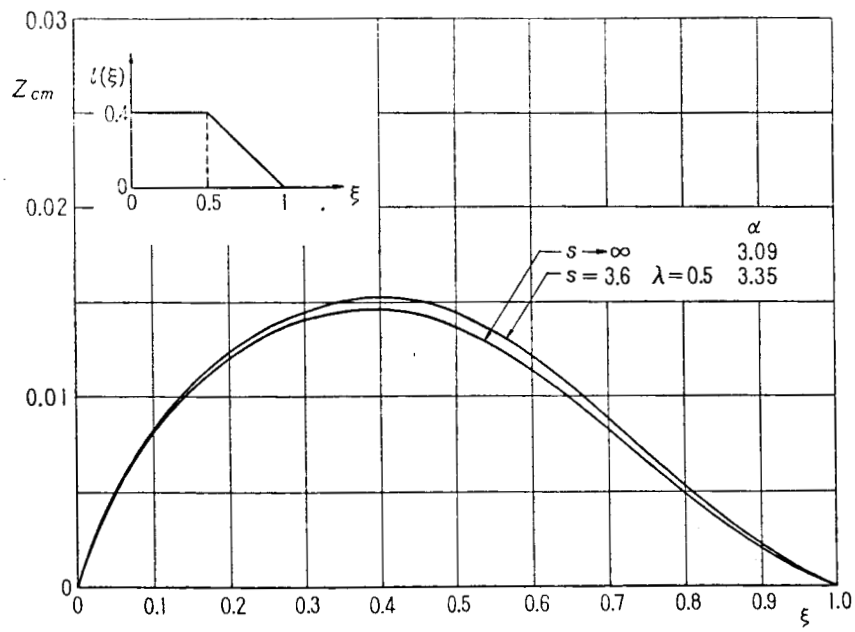

Figure 6 (b). Comparison of z_{cm} : y = 0.1

distribution affects z_{cm}. The maximum height is increased as the load distribution falls off towards the right.

Finally, Figure 11 is the vertical distribution of Mach numbers M_n for

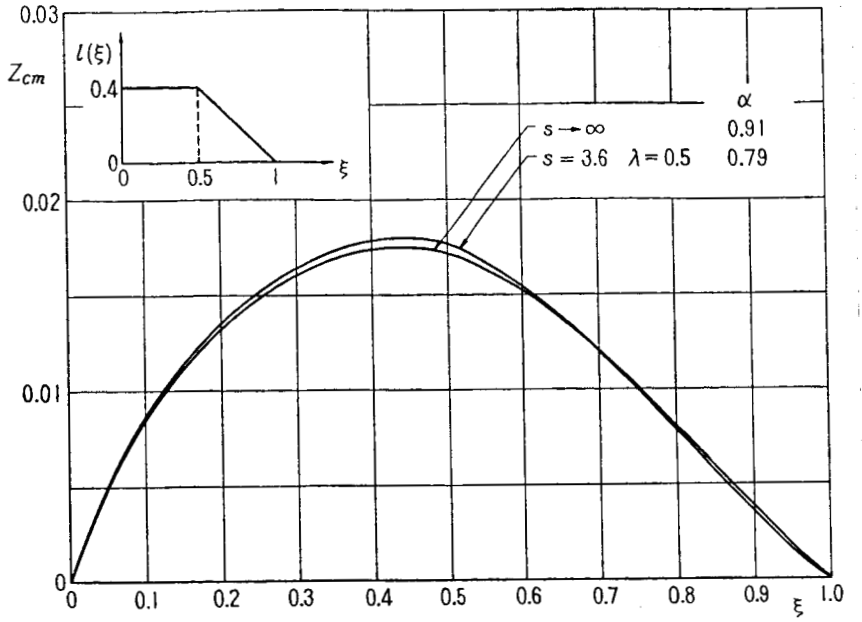

Figure 6 (c). Comparison of z_{cm} : y = 2

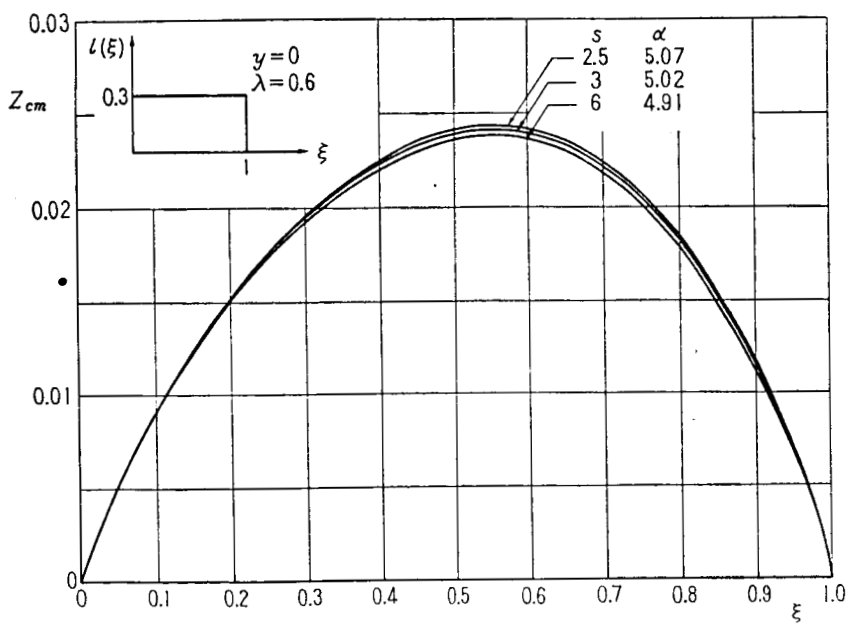

Figure 7. Variation of z_{cm} with s. /18

the case of s_c = 2.2, λ = 0.75 (A_r = 7) when the load distribution is $l(\xi)$ = = 0.4 x $l_1(\xi, 0)$ - 0.8 x $l_2(\xi, 0.5)$. The local Mach number M in the figure corresponds to the pressure coefficient $c_p = 1/2 \cdot l(\xi)$. As is clearly observed from the figure, the critical state is not reached yet as far as M_n is concerned

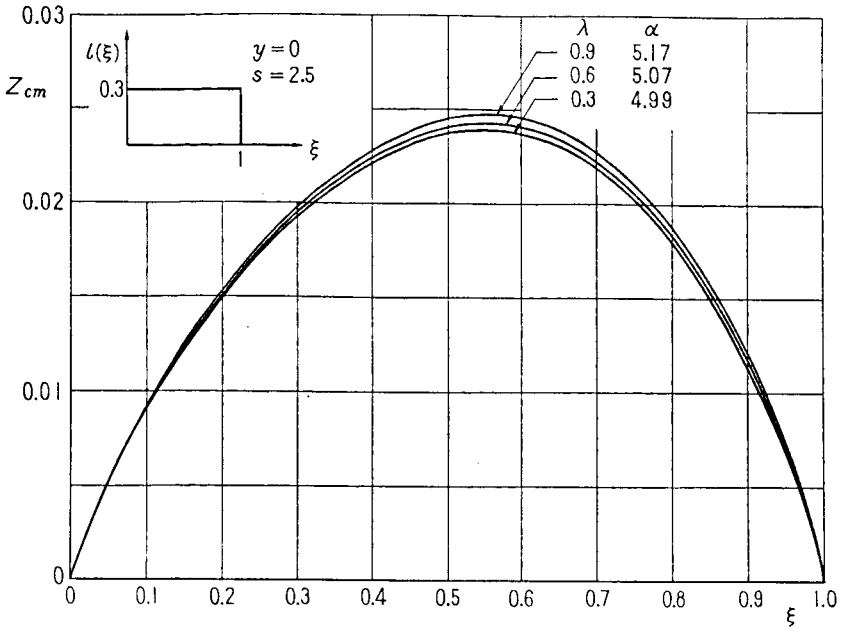

Figure 8. Variation of z_{cm} with λ.

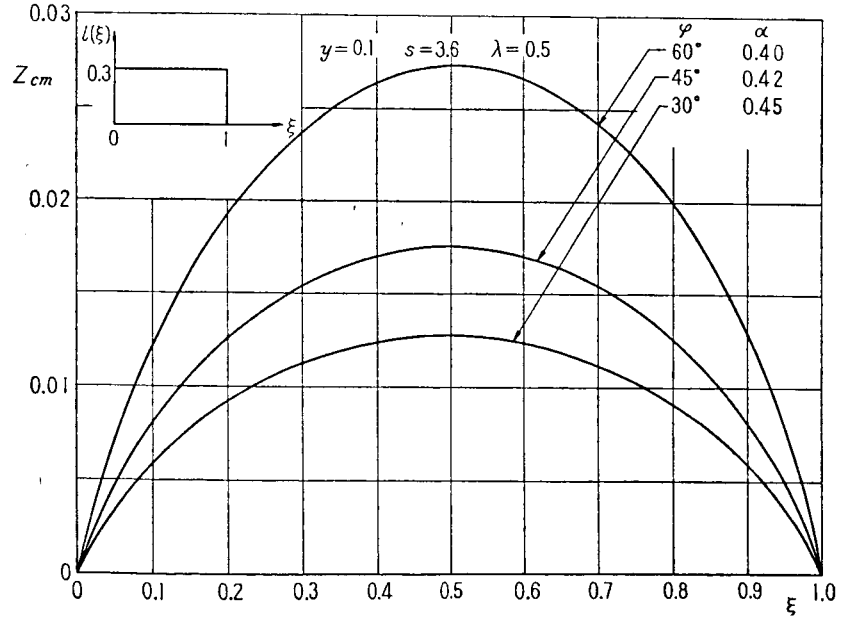

Figure 9. Variation of z_{cm} with Sweep-Back Angle.

when it becomes larger than 1. However, one has to be careful since the effect of wing thickness was not taken into account.

This M_n can be further reduced by taking into account the span-wise shape of the load distribution appropriately for the case of the same lift coefficient C_L.

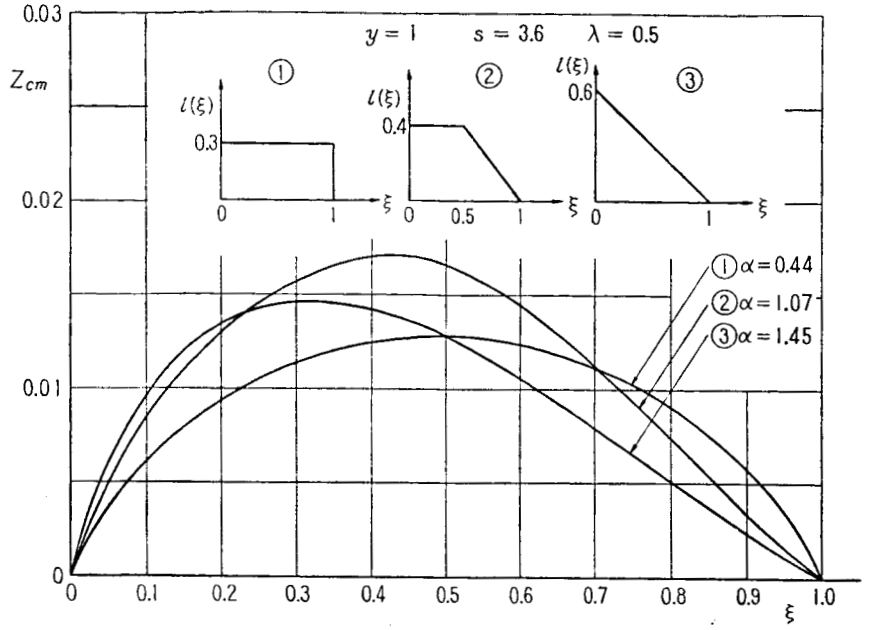

Figure 10. Variation of z_{cm} with Load Distribution

10. Conclusions

(1) The camber of a straight line taper wing having a span-wise uniform load distribution is obtained by means of the linear theory.

(2) The camber can be computed by deriving the velocity disturbance in the z-direction. In addition, equations of the disturbance potential and the velocity disturbances in the x- and y-directions are derived.

(3) The details of the flow field are found from the disturbance velocity. As an example, an equation giving the Mach number component normal to the isobars is derived.

(4) According to numerical computations, the camber variation is remarkable at the base and tip of the wing, but it is close to the shape of the two-dimensional case at the center. /21

(5) According to the numerical example of the Mach number component normal to the isobars, the reaching of the critical state in the flow field on the wing surface may be delayed by determining the camber so as to bring about a span-wise uniform distribution.

(6) The shape of the span-wise load distribution is arbitrary in principle. By an appropriate selection of this shape, an optimal shape of camber for the Mach number component normal to the isobars may be designed.

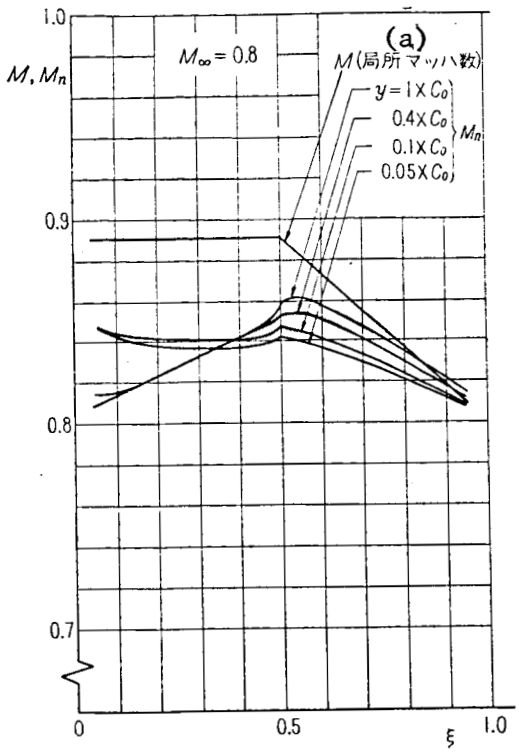

Figure 11 (a). Distribution of M_n : M_∞ = 0.8.
(a)-local Mach number

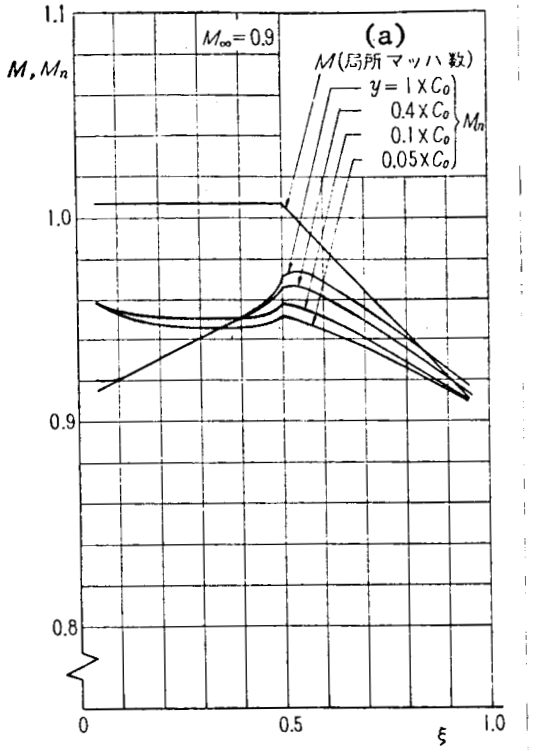

Figure 11 (b). Distribution of M_n: M_∞ = 0.9.
(a)-local Mach number

REFERENCES

1. Bickley, W. G. Critical Conditions for Compressible Flow, R & M 2330, 1946.
2. Küchemann, D., Weber, J., Brebner, G. G. Low Speed Tests on 45° Sweptback Wings, R & M 2882, 1951.
3. Küchemann, D., Weber, J. The Subsonic Flow Past Swept Wings at Zero Lift Without and With Body, R & M 2908, 1956.
4. Weber, J. The Shape of the Center Part of a Swept-back Wing with a Required Load Distribution, R & M 3098, 1957.
5. Lock, R. C. An Equivalence Law Relating Three- and Two-dimensional Pressure Distributions, R & M 3346, 1964.
6. Kawasaki, Toshio. "Semi-infinite Swept-Back Wing Having a Span-Wise Uniform Load Distribution". Aeronautical Technology Laboratory Report TR-94, 1965.

APPENDIX v_x and v_y

A. 1 $l_{1a}(\xi_1)=1(\xi_1-a)-1(\xi_1-1)$

$$8\pi\left(\frac{v_{xr1}}{V}\right)=\tan^{-1}\frac{[(s-y)^2+z^2]\tan\chi+x_{ra}(s-y)}{z\sqrt{x_{ra}{}^2+(s-y)^2+z^2}}-\tan^{-1}\frac{(y^2+z^2)\tan\chi-(x-a)y}{z\sqrt{(x-a)^2+y^2+z^2}}$$
$$-\tan^{-1}\frac{[(s-y)^2+z^2]\tan\psi+x_{r1}(s-y)}{z\sqrt{x_{r1}{}^2+(s-y)^2+z^2}}-\tan^{-1}\frac{(y^2+z^2)\tan\psi-(x-1)y}{z\sqrt{(x-1)^2+y^2+z^2}} \quad (A.1.1)$$

$$8\pi\left(\frac{v_{yr1}}{V}\right)=(1-a)\left\{\frac{z}{y^2+z^2}+\frac{(\lambda-1)z}{(s-y)^2+z^2}-\sigma\left(\tan^{-1}\frac{s-y}{z}+\tan^{-1}\frac{y}{z}\right)\right\}$$
$$-\tan\chi\left\{\tan^{-1}\frac{[(s-y)^2+z^2]\tan\chi+x_{ra}(s-y)}{z\sqrt{x_{ra}{}^2+(s-y)^2+z^2}}-\tan^{-1}\frac{(y^2+z^2)\tan\chi-(x-a)y}{z\sqrt{(x-a)^2+y^2+z^2}}\right\} \quad (A.1.2)$$
$$+\tan\psi\left\{\tan^{-1}\frac{[(s-y)^2+z^2]\tan\psi+x_{r1}(s-y)}{z\sqrt{x_{r1}{}^2+(s-y)^2+z^2}}-\tan^{-1}\frac{(y^2+z^2)\tan\psi-(x-1)y}{z\sqrt{(x-1)^2+y^2+z^2}}\right\}$$

and

$$v_{x1}=v_{xr1}(x,y,z)+v_{xr1}(x,-y,z) \quad (A.1.3)$$
$$v_{y1}=v_{yr1}(x,y,z)-v_{yr1}(x,-y,z) \quad (A.1.4)$$

A.2 $l_{2b}(\xi_1)=(\xi_1-b)[1(\xi_1-b)-1(\xi_1-1)]$ /22

$$8\pi\left(\frac{v_{xr2}}{V}\right)=\frac{\rho\sqrt{(x-\rho\tan\varphi)^2+(\rho-y)^2+z^2}}{(\rho-y)^2+z^2}z$$
$$\times\left\{\log\left|\frac{\sqrt{x_{r1}{}^2+(s-y)^2+z^2}-\sqrt{(x-\rho\tan\varphi)^2+(\rho-y)^2+z^2}+\sec\psi(s-\rho)}{\sqrt{x_{r1}{}^2+(s-y)^2+z^2}+\sqrt{(x-\rho\tan\varphi)^2+(\rho-y)^2+z^2}+\sec\psi(s-\rho)}\right|\right.$$
$$-\log\left|\frac{\sqrt{(x-1)^2+y^2+z^2}-\sqrt{(x-\rho\tan\varphi)^2+(\rho-y)^2+z^2}-\rho\sec\psi}{\sqrt{(x-1)^2+y^2+z^2}+\sqrt{(x-\rho\tan\varphi)^2+(\rho-y)^2+z^2}-\rho\sec\psi}\right|$$
$$-\log\left|\frac{\sqrt{x_{rb}{}^2+(s-y)^2+z^2}-\sqrt{(x-\rho\tan\varphi)^2+(\rho-y)^2+z^2}+\sec\Omega(s-\rho)}{\sqrt{x_{rb}{}^2+(s-y)^2+z^2}+\sqrt{(x-\rho\tan\varphi)^2+(\rho-y)^2+z^2}+\sec\Omega(s-\rho)}\right|$$
$$\left.+\log\left|\frac{\sqrt{(x-b)^2+y^2+z^2}-\sqrt{(x-\rho\tan\varphi)^2+(\rho-y)^2+z^2}-\rho\sec\Omega}{\sqrt{(x-b)^2+y^2+z^2}+\sqrt{(x-\rho\tan\varphi)^2+(\rho-y)^2+z^2}-\rho\sec\Omega}\right|\right\}$$
$$+\frac{\rho(x-\rho\tan\varphi)z}{2[(\rho-y)^2+z^2]}\left\{\log\left[\frac{\sqrt{x_{rb}{}^2+(s-y)^2+z^2}-x_{rb}}{\sqrt{x_{rb}{}^2+(s-y)^2+z^2}+x_{rb}}\cdot\frac{\sqrt{(x-b)^2+y^2+z^2}+x-b}{\sqrt{(x-b)^2+y^2+z^2}-(x-b)}\right]\right. \quad (A.2.1)$$
$$\left.-\log\left[\frac{\sqrt{x_{r1}{}^2+(s-y)^2+z^2}-x_{r1}}{\sqrt{x_{r1}{}^2+(s-y)^2+z^2}+x_{r1}}\cdot\frac{\sqrt{(x-1)^2+y^2+z^2}-(x-1)}{\sqrt{(x-1)^2+y^2+z^2}+x-1}\right]\right\}$$
$$+\frac{\rho[(\rho-y)(x-b-y\tan\Omega)+z^2\tan\Omega]}{(\rho-y)^2+z^2}$$
$$\times\left\{\tan^{-1}\frac{[(s-y)^2+z^2]\tan\Omega+x_{rb}(s-y)}{z\sqrt{x_{rb}{}^2+(s-y)^2+z^2}}-\tan^{-1}\frac{(y^2+z_2)\tan\Omega-(x-b)y}{z\sqrt{(x-b)^2+y^2+z^2}}\right\}$$
$$-\frac{\rho[(\rho-y)(x-1-y\tan\psi)+z^2\tan\psi]}{(\rho-y)^2+z^2}$$

$$\times\left\{\tan^{-1}\frac{[(s-y)^2+z^2]\tan\psi+x_{r1}(s-y)}{z\sqrt{x_{r1}^2+(s-y)^2+z^2}}-\tan^{-1}\frac{(y^2+z^2)\tan\psi-(x-1)y}{z\sqrt{(x-1)^2+y^2+z^2}}\right\}$$

$$-(1-a)\left\{\tan^{-1}\frac{[(s-y)^2+z^2]\tan\varphi+x_{r1}(s-y)}{z\sqrt{x_{r1}^2+(s-y)^2+z^2}}-\tan^{-1}\frac{(y^2+z^2)\tan\psi-(x-1)y}{z\sqrt{(x-1)^2+y^2+z^2}}\right\} \quad (A.2.1)$$

$$8\pi\left(\frac{v_{yr2}}{V}\right)=\frac{1}{2}(1-b)^2\left\{\frac{z}{y^2+z^2}+\frac{(\lambda-1)z}{(s-y)^2+z^2}-\sigma\left(\tan^{-1}\frac{s-y}{z}+\tan^{-1}\frac{y}{z}\right)\right\}$$

$$-\frac{\rho z}{2}\tan\Omega\left\{\frac{\sqrt{x_{rb}^2+(s-y)^2+z^2}}{(s-y)^2+z^2}-\frac{\sqrt{(x-b)^2+y^2+z^2}}{y^2+z^2}\right\}$$

$$+\left(1-a+\frac{\rho}{2}\sin\psi\right)z\left\{\frac{\sqrt{x_{r1}^2+(s-y)^2+z^2}}{(s-y)^2+z^2}-\frac{\sqrt{(x-1)^2+y^2+z^2}}{y^2+z^2}\right\}$$

$$+\frac{\rho(\rho-y)(x-\rho\tan\varphi)z}{[(\rho-y)^2+z^2]\sqrt{(x-\rho\tan\varphi)^2+(\rho-y)^2+z^2}}\left\{\frac{\rho(x-\rho\tan\varphi)\tan\varphi}{(\rho-y)^2+z^2}-1\right\}$$

$$\times\left\{\log\left|\frac{\sqrt{x_{rb}^2+(s-y)^2+z^2}-\sqrt{(x-\rho\tan\varphi)^2+(\rho-y)^2+z^2}+\sec\Omega(s-\rho)}{\sqrt{x_{rb}^2+(s-y)^2+z^2}+\sqrt{(x-\rho\tan\varphi)^2+(\rho-y)^2+z^2}+\sec\Omega(s-\rho)}\right|\right. \quad /23$$

$$-\log\left|\frac{\sqrt{(x-b)^2+y^2+z^2}-\sqrt{(x-\rho\tan\varphi)^2+(\rho-y)^2+z^2}-\rho\sec\Omega}{\sqrt{(x-b)^2+y^2+z^2}+\sqrt{(x-\rho\tan\varphi)^2+(\rho-y)^2+z^2}-\rho\sec\Omega}\right|$$

$$-\log\left|\frac{\sqrt{x_{r1}^2+(s-y)^2+z^2}-\sqrt{(x-\rho\tan\varphi)^2+(\rho-y)^2+z^2}+\sec\varphi(s-\rho)}{\sqrt{x_{r1}^2+(s-y)^2+z^2}+\sqrt{(x-\rho\tan\varphi)^2+(\rho-y)^2+z^2}+\sec\varphi(s-\rho)}\right|$$

$$\left.+\log\left|\frac{\sqrt{(x-1)^2+y^2+z^2}-\sqrt{(x-\rho\tan\varphi)^2+(\rho-y)^2+z^2}-\rho\sec\psi}{\sqrt{(x-1)^2+y^2+z^2}+\sqrt{(x-\rho\tan\varphi)^2+(\rho-y)^2+z^2}-\rho\sec\psi}\right|\right\}$$

$$+\frac{\rho(\rho-y)z}{2[(\rho-y)^2+z^2]}\left\{\frac{(x-\rho\tan\varphi)^2}{(\rho-y)^2+z^2}+\frac{1}{2}\right\} \quad (A.2.2)$$

$$\times\left\{\log\left[\frac{\sqrt{x_{rb}^2+(s-y)^2+z^2}-x_{rb}}{\sqrt{x_{rb}^2+(s-y)^2+z^2}+x_{rb}}\cdot\frac{\sqrt{(x-b)^2+y^2+z^2}+x-b}{\sqrt{(x-b)^2+y^2+z^2}-(x-b)}\right]\right.$$

$$\left.-\log\left[\frac{\sqrt{x_{r1}^2+(s-y)^2+z^2}-x_{r1}}{\sqrt{x_{r1}^2+(s-y)^2+z^2}+x_{r1}}\cdot\frac{\sqrt{(x-1)^2+y^2+z^2}+x-1}{\sqrt{(x-1)^2+y^2+z^2}-(x-1)}\right]\right\}$$

$$+\frac{\rho}{2[(\rho-y)^2+z^2]}\left\{\frac{(\rho-y)^2-z^2}{(\rho-y)^2+z^2}(x-\rho\tan\varphi)^2-z^2\right\}$$

$$\times\left\{\tan^{-1}\frac{[(s-y)^2+z^2]\tan\Omega+x_{rb}(s-y)}{z\sqrt{x_{rb}^2+(s-y)^2+z^2}}-\tan^{-1}\frac{(y^2+z^2)\tan\Omega-(x-b)y}{z\sqrt{(x-b)^2+y^2+z^2}}\right.$$

$$\left.-\tan^{-1}\frac{[(s-y)^2+z^2]\tan\psi+x_{r1}(s-y)}{z\sqrt{x_{r1}^2+(s-y)^2+z^2}}+\tan^{-1}\frac{(y^2+z^2)\tan\psi-(x-1)y}{z\sqrt{(x-1)^2+y^2+z^2}}\right\}$$

$$+\left\{(1-b)\tan\psi+\frac{\rho}{2}\tan^2\psi\right\}$$

$$\times\left\{\tan^{-1}\frac{[(s-y)^2+z^2]\tan\psi+x_{r1}(s-y)}{z\sqrt{x_{r1}^2+(s-y)^2+z^2}}-\tan^{-1}\frac{(y^2+z^2)\tan\psi-(x-1)y}{z\sqrt{(x-1)^2+y^2+z^2}}\right\}$$

$$-\frac{\rho}{2}\tan^2\Omega\left\{\tan^{-1}\frac{[(s-y)^2+z^2]\tan\Omega+x_{rb}(s-y)}{z\sqrt{x_{rb}^2+(s-y)^2+z^2}}-\tan^{-1}\frac{(y^2+z^2)\tan\Omega-(x-b)y}{z\sqrt{(x-b)^2+y^2+z^2}}\right\}$$

Similarly to (A.1.3) and (A.1.4):

$$v_{x2}=v_{xr2}(x,y,z)+v_{xr2}(x,-y,z) \quad (A.2.3)$$

$$v_{y2}=v_{yr2}(x,y,z)-v_{yr2}(x,-y,z) \quad (A.2.4)$$